Influence de la circulation à grande échelle sur le transfert de chaleur en convection turbulente rugueuse

Influence of wind on heat transfer in turbulent convection with roughness

Nathan CARBONNEAU[1,2], **Julien SALORT**[3], **Yann FRAIGNEAU**[1], **Anne SERGENT**[1,4*]

[1] Laboratoire Interdisciplinaire des Sciences du Numérique
Université Paris-Saclay, CNRS, Orsay (France)
[2] Sorbonne Université, Collège Doctoral, Paris (France)
[3] Laboratoire de Physique
Ecole Normale Supérieure de Lyon, CNRS, Lyon (France)
[4] Sorbonne Université, Faculté des Sciences et Ingénierie, Paris (France)
*(Corresponding author: anne.sergent@lisn.fr)

Résumé - Des simulations numériques directes 3D sont réalisées en configuration de Rayleigh-Bénard confinée et périodique pour un nombre de Rayleigh de 10^{10}. La plaque inférieure est soit lisse, soit rugueuse. Les domaines périodiques visent à reproduire les petites structures du cœur de la cavité, mais sans le cisaillement dû au vent de la circulation à grande échelle. Par comparaison des cas confinés et périodiques, l'effet du vent est mis en évidence. On montre que dans le cas lisse, le transfert de chaleur est indépendant de la présence du vent. Contrairement à ce qui est communément admis, l'augmentation du transfert de chaleur par la rugosité ne repose qu'en partie sur les interactions vent - rugosité, et uniquement lorsque la rugosité émerge au-dessus des couches limites thermique et visqueuse.

Abstract - Direct 3D numerical simulations are carried out in periodic and confined Rayleigh-Bénard cases for a Rayleigh number equal to 10^{10}. The lower plate is either smooth or rough. Periodic domains aim to reproduce the small structures of the cavity core without the wind-induced shear of the large-scale circulation. A comparison of confined and periodic cases highlights the effect of wind. It is shown that in the smooth case, heat transfer is independent of the wind presence. Contrary to the common hypothesis, the increase in heat transfer due to roughness is only partly based on wind-roughness interactions, and only when roughness emerges above the thermal and viscous boundary layers.

Nomenclature

H	domain height, m
g	gravity acceleration, $\mathrm{m/s^2}$, $\mathbf{g} = -g\mathbf{e_z}$
h_p	dimensionless block height
k_x	dimensionless wave number
t	dimensionless time unit
Γ_i	aspect ratios ($i = x, y$)
α	thermal expansion coefficient, K^{-1}
θ	dimensionless temperature
κ	thermal diffusivity, $\mathrm{m^2/s}$
λ_p	dimensionless roughness length-scale
ν	kinetic viscosity, $\mathrm{m^2/s}$
τ	turnover time, $\tau = \pi\ (Ra/Pr)^{1/2}/Re_{LSC}$
Ra	Rayleigh number, $Ra = \alpha g \Delta T H^3/(\nu\kappa)$
Pr	Prandtl number, $Pr = \nu/\kappa$
Nu	Nusselt number
Re	Reynolds number
$\mathbf{u} = (u, v, w)$	dimensionless velocity vector
$\mathbf{x} = (x, y, z)$	dimensionless coordinates
$< . >_t$	time average
$< . >_{x,y}$	average over horizontal plane
$(.)'$	time-fluctuations

https://doi.org/10.25855/SFT2025-112

1. Introduction

Natural convection is ubiquitous in both industrial and natural fluid flows. An ideal model is the Rayleigh-Bénard convection (RBC): a fluid layer heated from below and cooled from above. One or several convection cells can appear called Large Scale Circulation (LSC) and the wind is the mean horizontal component of the LSC along the upper and lower plates . The RBC inside a closed cavity or within large periodic domains has been extensively studied (see [1] for a review). Nevertheless, in nature, underlying surfaces are not ideal in terms of surface condition. In some studies, wall roughness has been added either on one or both plates. Its effect on heat transfer across the domain is far from negligible. Three heat transfer regimes have been identified based on the relative kinetic and thermal boundary layer thicknesses compared to roughness height [2, 3]. However, the mechanisms leading to such a change are still poorly understood [4]. In particular, interactions between wall roughness and the horizontal wind are thought to play a key role in the heat transfer modification [5, 6].

To improve the knowledge of the interactions between wind and roughness, we consider a particular configuration in which wind is negligible compared to the other flow components. In this study, we performed 3D DNS simulations of flows in cavities with a smooth or rough bottom plate while the top plate remains smooth. These simulations of confined cavities are considered as a reference to be compared with a windless configuration inside slender periodic layers , in which the LSC cannot settle. The wind effect on small structures and heat transfer is highlighted by comparing the reference flow in cavities (with LSC) with that obtained in periodic layers (without LSC).

The paper is organized as follows: Section 2 introduces the physical problem and the numerical setup. Section 3 presents the global flow structure in confined and periodic configurations. Finally, the wind effect on both the heat transfer in smooth and rough cases and on small structure sizes is described in Section 4.

2. Physical configuration and governing equations

2.1. Physical set-up

We study the natural convection flow inside smooth or rough Rayleigh-Bénard rectangular confined cavities or periodic layers. The cold top plate (respectively, the hot bottom plate that may include roughness) is isothermal at constant temperature T_c (respectively T_h). No-slip conditions are imposed on the walls. The geometric aspect ratios are defined as $\Gamma_x = L_x/H$ and $\Gamma_y = L_y/H$, where H is the height of the domain and L_x and L_y are the horizontal sizes.

Rough configurations are asymmetric, with roughness applied exclusively to the bottom plate. The roughness is modelled using a series of square blocks. The fluid space around blocks is referred to as a valley. The block distribution on the plate is uniform. The roughness pattern in each horizontal direction is fully described by the roughness length-scale λ_p and the block width w_p as $\lambda_p = w_p + w_v$, with w_v the valley width ($w_v = w_p$). Two roughness heights (h_p) are chosen. In both cases, the block width is set to maintain a constant aspect ratio w_p/h_p equal to 2.5. It is well known that three different regimes of heat transfer exist in a rough cavity as a function of the height of roughness relative to the thickness of the boundary layers (see [2, 3] for example). Regime I corresponds to a flow where the roughness is included in both thermal and kinetic boundary layers, resulting in a reduction of the heat transfer compared to

the smooth case. In regime II, the roughness is sandwiched between the two boundary layers associated with efficient heat transfer with a scaling law in $Ra^{1/2}$. Finally the blocks exceed the two boundary layers in the regime III and the heat transfer scales in $Ra^{1/3}$. Here, the test cases RS2 belong to regime II, while the RS3 configurations belong to regime III (see table 1).

In cavity cases, the vertical sidewalls are adiabatic. In contrast, in periodic fluid layers, periodic conditions are applied in two horizontal directions, both on temperature and velocity fields. In periodic configurations, Γ_x and Γ_y are smaller than in cavities but large enough to allow the existence of turbulent structures of sizes comparable to those observed in a cavity, the size of the LSC not being taken into account. To prevent favouring one of the two horizontal directions in periodic domains, only square-based periodic domains are considered. Nevertheless, we had to slightly modify the size of the domains used in the rough cases so that an integer number of rough patterns could be modelled (see table 1).

The physical parameters describing the problem are the Rayleigh number (Ra) and the Prandtl number (Pr). The Rayleigh number is set to 10^{10}. The working fluid is water at a mean temperature of 40° C, so the Prandtl number is set to 4.4.

The response of the system is twofold and corresponds i) to the heat transfer in the cavity, measured in terms of the Nusselt number (Nu, eq. 1), and ii) to the intensity of the LSC that is established in the cavity, measured in terms of the Reynolds numbers (Re): the Reynolds number based on the time-averaged horizontal velocity (Re_{LSC}) and the turbulent Reynolds number (Re_{RMS}) based on the fluctuations of the horizontal velocity. It can be noticed that definitions (eq. 2, 3) are based on the maximum values over the cavity height. The definitions below are consistent with the characteristic quantities employed to make the flow equations dimensionless, as defined in the section 2.2.

$$Nu(\mathbf{x},t) = \sqrt{RaPr}\, w(\mathbf{x},t)\theta(\mathbf{x},t) - \partial_z \theta(\mathbf{x},t), \tag{1}$$

$$Re_{LSC} = \sqrt{Ra/Pr}\ \max\left\{ \sqrt{\left\langle \langle u\rangle_t^2 + \langle v\rangle_t^2 \right\rangle_{x,y}} : z \right\}, \tag{2}$$

$$Re_{RMS} = \sqrt{Ra/Pr}\ \max\left\{ \sqrt{\left\langle u_{RMS}^2 + v_{RMS}^2 \right\rangle_{x,y}} : z \right\} \tag{3}$$

As we focus on the shear of plumes by the wind (far from the corner flows), the Reynolds number in the cavity is calculated using a spatial averaging on a restricted horizontal plane: $(x,y) \in [0.2;0.8] \times [0.15,0.35]$. It is worth noting that no such horizontal restriction exists in periodic configurations.

2.2. Governing equations and Numerical methods

The Navier-Stokes equations under the Boussinesq approximation are solved using a finite volume approach employing the in-house SUNFLUIDH solver. The reader is referred to the work of [3] for a complete description and validation of the solver in the turbulent Rayleigh-Bénard case, including rough configurations. The dimensionless form of the equations is written as follows, considering the domain height H, the temperature difference ΔT and the free-fall velocity $\kappa\sqrt{RaPr}/H$ as references:

$$\nabla \cdot \mathbf{u} = 0, \tag{4}$$

$$\partial_t \mathbf{u} + \mathbf{u}\cdot\nabla\mathbf{u} = -\nabla P^* + \sqrt{Pr/Ra}\,\nabla^2\mathbf{u} + \theta\mathbf{e_z}, \tag{5}$$

$$\partial_t \theta + \mathbf{u}\cdot\nabla\theta = 1/\sqrt{PrRa}\,\nabla^2\theta \tag{6}$$

Case	$\Gamma_x \times \Gamma_y$	h_p	$N_x \times N_y \times N_z$	τ	Δt	N_τ
Cavity configurations						
C-SS	1×0.5	-	$1024 \times 768 \times 1280$	34.9	293	8.4
C-RS2	1×0.5	0.004	$1536 \times 768 \times 1152$	23.9	100	4.2
C-RS3	1×0.5	0.03	$1056 \times 512 \times 1056$	28.5	114	4.0
Periodic configurations						
P-SS	0.44×0.38	-	$448 \times 380 \times 1280$	-	154	-
P-RS2	0.44×0.38	0.004	$704 \times 576 \times 1152$	-	98	-
P-RS3	0.45×0.375	0.03	$384 \times 384 \times 1056$	-	159	-

Table 1: *DNS parameters for $Ra = 10^{10}$ and $Pr = 4.4$: the number N_i of cells in the direction $\vec{e}_i$ ($i = (x,y,z)$); the time period for statistics Δt ; the turnover time τ if any ; the number of LSC turnovers N_τ. τ is not defined in the periodic cases due to the loss of LSC (see section 3).*

Cases	C-SS	C-RS2	C-RS3	P-SS	P-RS2	P-RS3
Nu	129.3 ± 0.2	145.3 ± 0.3	168.6 ± 0.2	129.6 ± 0.9	145.1 ± 1.6	162.7 ± 1.7
Re_{LSC}	5330	6270	6020	554	838	617
Re_{RMS}	3190	2730	2770	2460	2800	2620

Table 2: *The mean Nusselt number Nu and its standard deviation; the Reynolds numbers (Re_{LSC} and Re_{RMS}) based on the mean LSC or its fluctuations (see eq. 2, 3).*

where P^* is the driving pressure. The temperature of the top cold plate is taken as a reference so that the dimensionless temperature θ ranges between $\theta_c = 0$ and $\theta_h = 1$.

The mesh size is chosen to be smaller than the Kolmogorov scale. A sufficient number of cells is set inside thermal and kinetic boundary layers to match the criteria by [7]. In periodic configurations, the same mesh as in the corresponding cavity configurations is applied (same *Ra* number and same bottom wall condition).

The spatial and temporal convergence of the simulations was assessed using time-averaged Nusselt numbers calculated using different methods (spatial averages on horizontal planes or by volume) as proposed by [7]. The Nusselt numbers calculated from the volume averages of dissipation rates are not considered with regard to the difficulty of getting accurate volume averages inside valleys. Convergence with a deviation of less than 1% is achieved over the simulated time interval. In the cavity configuration, the simulated time interval can be measured in terms of turnover time τ, that corresponds to the time required for the LSC to complete one revolution within the cavity. All the simulation details can be found in Table 1.

3. Large scale circulation and periodic domains

The specific nature of this study is that narrow periodic fluid layers are considered, which are less than half the size of the cavity. We focus here on the flow organization, and in particular, the large-scale circulation described by the two Reynolds numbers (eq. 2, 3).

Comparing values of Re_{LSC} for similar configurations in table 2, it appears that the *LSC* intensity is negligible in the periodic configurations, as Re_{LSC} is around one order of magnitude smaller in periodic cases than in the corresponding reference cavities. At the same time, Re_{RMS} remains broadly similar, whatever the geometry. This means that the large-scale flow has van-

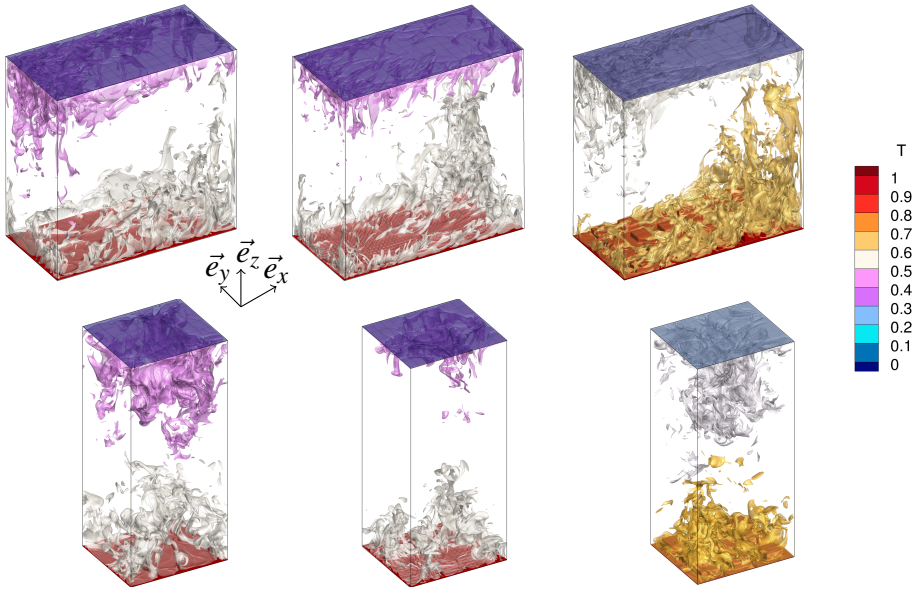

Figure 1: *Instantaneous temperature field for cavities (C- cases, top), and periodic configurations (P- cases, bottom). Left: C-SS and P-SS cases, middle: C-RS2 and P-RS2 cases, right: C-RS3 and P-RS3 cases.*

ished in the periodic fluid layer, although horizontal fluctuations remain present, probably due to disturbances caused by the plume sweeping. In particular, in all periodic configurations, horizontal fluctuations dominate the intensity of the LSC ($Re_{LSC} \ll Re_{RMS}$). This phenomenon is illustrated in Fig. 1. In periodic configurations, hot and cold plumes fill the whole domain and move upwards or downwards (respectively) across the bulk. In cavities, on the other hand, the plumes are tilted by the wind and pushed towards the walls, creating jets along the vertical walls. The periodic domains are too small for an LSC to be established.

To conclude, the direct comparison between flows in cavities (with LSC) and in narrow periodic layers (without LSC) can be viewed as a good candidate to investigate the flow organization when shear is missing and how the wind alters the small, turbulent structures and the nature of the heat transfer.

4. Wind effect on the turbulent convection

A general point of view is given by considering the average Nusselt number (Nu) to measure the overall heat transfer across the fluid volume. As expected, adding roughness on a plate significantly increases the global heat transfer (see table 2). Moreover, in the SS and RS2 cases, Nu remains nearly constant regardless of the confinement (cavity C- or periodic P- configurations). In contrast, in the RS3 cases, Nu decreases by 3.5% when the shear is missing. This suggests that the wind is involved in the heat transfer in regime III, but that another mechanism leads to the large heat transfer increase linked to roughness.

However, in all cases, heat is transported by small flow structures, such as plumes. To evaluate how the wind modifies the energy distribution across different scales, the power spectra of temperature fluctuations and turbulent heat flux are computed along the x direction for altitudes z comprised in the half-bottom domain and averaged in time (Fig. 2). This quantity is related to

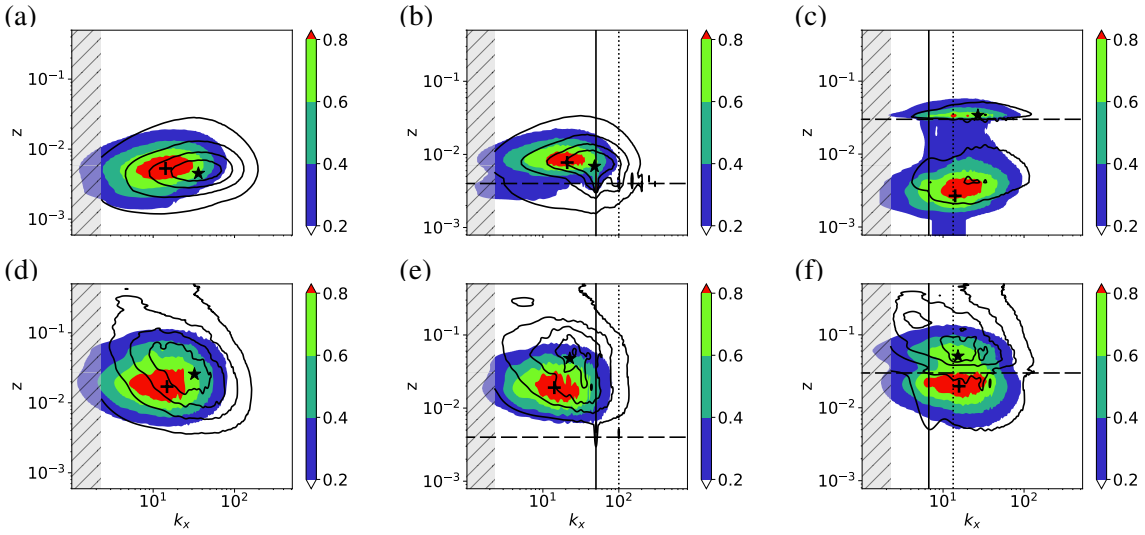

Figure 2: *The premultiplied temperature power spectrum $k_x E_{\theta'\theta'}$ (top) and the premultiplied heat flux co-spectrum $k_x E_{w'\theta'}$ (bottom) normalized by the maximum density value of each case, where k_x is the wavenumber in the horizontal direction e_x and computed in the bottom half of the domain at $y = \Gamma_y/2$. The three geometrical configurations are displayed: (left) SS cases; (middle) RS2 cases; (right) RS3 cases. Colours correspond to the cavity cases and lines to the periodic configurations. The grey shaded areas correspond to the unreachable k_x in the periodic configurations because of the reduced size of the domain. The solid (resp. dashed and dotted) line corresponds to $k_p = 1/\lambda_p$ (resp. h_p and $k_v = 1/w_v$). Marker + (resp. $\star$) points to the peak location of the spectral density in the cavity (resp. in periodic configurations).*

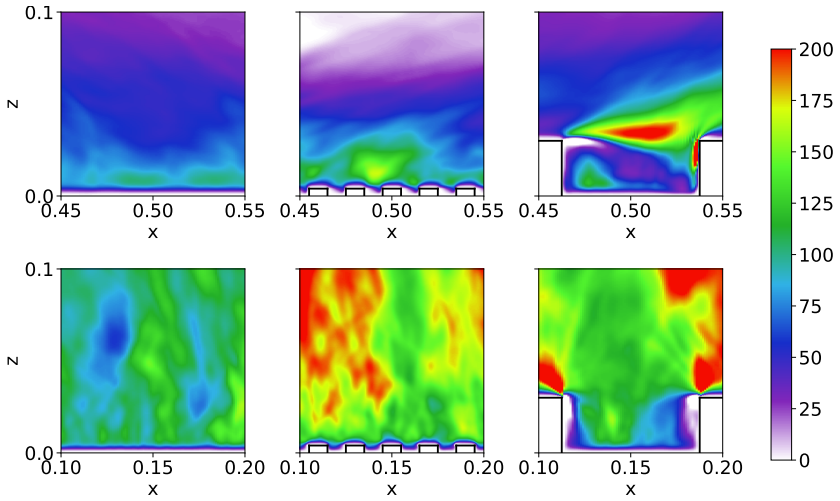

Figure 3: *Local time-averaged turbulent Nusselt number ($\sqrt{RaPr}\langle w'\theta'\rangle_t$) in the vertical mid-plane. Cavity cases (top); periodic configurations (bottom); SS cases (left); RS2 cases (middle) and RS3 cases (right).*

the RMS fluctuations of the considered field χ as $\chi^2_{rms} = \int_0^{+\infty} k_x E_{\chi'\chi'} d(\log k_x)$.

Figs. 2a, 2b, 2d and 2e display the temperature power spectrum and the heat flux co-spectrum in the cases SS and RS2. Both have similar responses to the wind. A clear peak is present in altitude $z \lessapprox 0.01$ in the range $k_x \approx 14(21)$ for C-SS (C-RS2, respectively) and $k_x \approx 36(47)$ for P-SS (P-RS2, resp.). It illustrates that the thermal structures (plumes) tend intrinsically to be smaller when the wind is missing. A weak imprint of the roughness pattern can be noticed on θ in the case RS2 (Fig. 2b). For C-SS and C-RS2 cases, an oblong shape with a horizontal axis is recovered for the $k_x E_{w'\theta'}$ co-spectrum in the same way as for temperature, but for slightly higher z. In contrast, the intrinsic shape associated with windless heat transfer is a tilted ellipsoid with a negative slope corresponding to the natural clustering of plumes: the most energetic structures become larger with the altitude z. In the case of cavities, the plumes remain mostly confined to the mixing layer (first 1/10th of the height), while in periodic cases, the plumes continue to grow up to the core of the cavity.

The case RS3 (Figs. 2c and 2f) is very different. Two peaks appear in cavities: one inside the valley and a second just above roughness (but to a lesser magnitude for heat flux co-spectrum). These peaks are located at a k_x larger than the valley wavenumber (k_v) and at the base of the valley for temperature or at the upper interface for heat flux, showing that temperature structures and the most intense heat transfer fluctuations are intrinsically linked to the flow inside valleys or above blocks. When the wind is removed (P-RS3), the $k_x E_{\theta'\theta'}$ spectrum is nearly unchanged, with a maximum density associated with smaller length scales than in cavity, and mainly above the roughness height, instead of below. $k_x E_{w'\theta'}$ co-spectrum (Fig. 2f) shows that the most intense fluctuations occur close to the upper interface of valleys in both cases (below with wind or above without) but at an unchanged wavenumber equal to the k_v. At higher altitudes, we find the tilted ellipsoid characterising the grouping of plumes. This indicates a wind-induced change in the flow dynamics in the valleys in rough regime III.

To make these differences of pattern and peak location in the $k_x E_{w'\theta'}$ co-spectra clearer, we consider the mean fields of turbulent heat transfer (Fig. 3). The shear of the plumes is distinctly observed for the SS and RS2 cases, while the near-wall area remains unchanged. In contrast, two different thermal transfer mechanisms can be observed in the RS3 cases with or without wind. In the windless case (P-RS3), plumes stick all around the solid blocks. In contrast, in the C-RS3, at the upper interface of the valley, a turbulent heat flux emerges from the upstream solid block and is deviated by the wind, creating a mixing layer developing in the wind direction and impacting the opposite solid block, where intense heat flow occurs. This mixing mechanism is particularly efficient in transferring heat and consequently increases Nu when shear is present.

5. Conclusion

DNS results of turbulent RBC are presented for water-filled cavities and periodic layers in smooth and asymmetric rough configurations. The horizontal size of the periodic layers was determined in such a way as to allow the small structures typical of those found inside the cores of RB cavities to become established. Firstly, an examination of the Reynolds numbers shows that the retained horizontal size of the periodic layers is too small for wind to be present. In all periodic cases, the Re_{LSC} based on the LSC has become negligible compared to the Re_{RMS} based on the wind fluctuations, although wind fluctuations keep the same order of magnitude as in the cavity. As a result, the resulting windless periodic configurations provide a comparison case for assessing the effect of wind inside cavities.

In the smooth case (SS) and in the rough regime II (RS2), the wind tends to increase the

size of small structures (thermal or related to heat transfer). But it also breaks down the natural aggregation of plumes by confining the most energetic structures to the outer zone of the thermal boundary layer. Surprisingly, *Nu* is unchanged when the periodic and the cavity cases are compared. This agrees with previous studies suggesting that *Nu* is insensitive to the wind intensity [9, 10] in the classic smooth RBC. However, we can even state that *Nu* is insensitive to the existence of the wind itself. Moreover, the commonly admitted hypothesis that the wind-roughness interaction is responsible for the Nusselt number increase in rough configurations [5, 6] needs to be mitigated. As explained above, in the rough regime II, *Nu* is insensitive to the wind. But in the rough regime III, the wind-roughness interaction is responsible for a small part of the Nusselt number increase (around 15%). This increase in heat transfer is the result of a noticeable change in the fluid flow above the rough valleys: the wind causes a mixing layer to appear above the valley, which impacts the windward face of the next block, while in the wind absence, plumes envelop solid blocks. This phenomenon explains why, whatever the confinement, scales associated with the heat transfer remain of the order of the valley size. Consequently, the wind-roughness interaction hypothesis having been disproved by this study, the mechanism responsible for all (regime II) or most (regime III) of the increase in heat transfer due to roughness has yet to be fully elucidated.

However, these conclusions must be taken cautiously, as only one Rayleigh number is studied with a single shape and arrangement of rough elements. Further investigations are needed to confirm these results over a wider range of parameters (*Ra*, *Pr*, roughness parameters).

Acknowledgements

This work benefits from the French National Research Agency funding (ANR-22-CE30-0018-02). The DNS database has been built using granted access to the HPC resources of TGCC under allocation 2a0326 made by GENCI.

References

[1] F. Chillà et al., New Perspectives in Turbulent Rayleigh-Bénard Convection, *Eur. Phys. J. E*, 35-7 (2012) 58.

[2] Y.-C. Xie et al., Turbulent thermal convection over rough plates with varying roughness geometries, *J. Fluid Mech.*, 825 (2017) 573-599.

[3] M. Belkadi et al., On the role of roughness valleys in turbulent Rayleigh–Bénard convection, *J. Fluid Mech.*, 923 (2020) A6.

[4] O. Liot et al., Velocity fluctuations and boundary layer structure in a rough Rayleigh-Bénard cell filled with water, *Phys. Rev. Fluids*, 2-4 (2018) 044605.

[5] Y.-B. Du et al., Turbulent thermal convection in a cell with ordered rough boundaries, *J. Fluid Mech.*, 407 (2000) 57-84.

[6] H. Jiang et al., Controlling Heat Transport and Flow Structures in Thermal Turbulence Using Ratchet Surfaces, *Phys. Rev. Lett.*, 120-4 (2018) 044501.

[7] O. Shishkina et al., Boundary layer structure in turbulent thermal convection and its consequences for the required numerical resolution, *New J. Phys.*, 12-7 (2010) 075022.

[8] A. Parodi et al., Clustering of Plumes in Turbulent Convection, *Phys. Rev. Lett.*, 92-19 (2004) 194503.

[9] P.-E. Roche et al., On the triggering of the Ultimate Regime of convection, *New J. Phys.*, 12-8 (2010) 085014.

[10] G. Ahlers et al., Heat transfer and large scale dynamics in turbulent Rayleigh-Bénard convection, *Rev. Mod. Phys.*, 81-2 (2009) 503-537.